JBC Papers in Press. Published on June 24, 2019 as Manuscript RA119.008902
The latest version is at http://www.jbc.org/cgi/doi/10.1074/jbc.RA119.008902

Tick saliva protein Evasin-3 modulates chemotaxis by disrupting CXCL8 interactions with glycosaminoglycans and CXCR2

Stepan S. Denisov[1], Johannes H. Ippel[1], Alexandra C.A. Heinzmann[1], Rory R. Koenen[1], Almudena Ortega-Gomez[2], Oliver Soehnlein[2,3,4,5], Tilman M. Hackeng[1], Ingrid Dijkgraaf[1]*

[1]Department of Biochemistry, University of Maastricht, Cardiovascular Research Institute Maastricht (CARIM), Universiteitssingel 50, 6229 ER, Maastricht, The Netherlands

[2]Institute for Cardiovascular Prevention (IPEK), Ludwig Maximilian University, Pettenkoferstraße 8a, 80336, Munich, Germany

[3]German Center for Cardiovascular Research (DZHK), Oudenarder Straße 16, 13316, Berlin, Germany

[4]Partner Site Munich Heart Alliance, Munich, Germany

[5]Department of Physiology and Pharmacology (FyFa) and Department of Medicine, Karolinska Institutet, SE-171 77, Stockholm, Sweden

Running title: Evasin-3-based peptides modulate chemotaxis by CXCL8 binding

*Ingrid Dijkgraaf: Department of Biochemistry, University of Maastricht, Cardiovascular Research Institute Maastricht (CARIM), Universiteitssingel 50, 6229 ER, Maastricht, The Netherland; i.dijkgraaf@maastrichtuniversity.nl

Keywords: chemokine, peptide chemical synthesis, parasite, nuclear magnetic resonance (NMR), protein structure, C-X-C motif chemokine ligand (CXCL)

Abstract

Chemokines are a group of chemotaxis proteins that regulate cell trafficking and play important roles in immune responses and inflammation. Ticks are blood-sucking parasites that secrete numerous immune-modulatory agents in their saliva to evade host immune responses. Evasin-3 is a small salivary protein which belongs to a class of chemokine-binding proteins isolated from the brown dog tick, *Rhipicephalus sanguineus*. Evasin-3 has been shown to have a high affinity for chemokines CXCL1 and CXCL8 and diminish inflammation in mice. In the present study, solution NMR spectroscopy was used to investigate the structure of Evasin-3 and its CXCL8/Evasin-3 complex. Evasin-3 is found to disrupt the glycosaminoglycan (GAG) binding site of CXCL8 and inhibit the interaction of CXCL8 with CXCR2. Structural data were used to design two novel CXCL8 binding peptides. Linear tEv3 17-56 and cyclic tcEv3 16-56 dPG Evasin-3 variants were chemically synthesized by solid phase peptide synthesis. Affinity of these newly synthesized variants to CXCL8 were measured by surface plasmon resonance (SPR) biosensor analysis. Kd values of tEv3 17-56 and tcEv3 16-56 dPG were 27 and 13 nM, respectively. Both compounds effectively inhibited CXCL8 induced migration of polymorphonuclear neutrophils (PMN). The present results suggest utility of synthetic Evasin-3 variants as scaffolds for designing and fine-tuning new chemokine-binding agents that suppress immune responses and inflammation.

Introduction

Chemokines are a diverse group of chemotaxis proteins which guide cell trafficking and play an important role in diverse physiological processes such as immune response, inflammation, angiogenesis, and cell differentiation (1). Although chemokines structurally fall into two

major (CC and CXC) and two minor (XC and CX3C) groups depending on their cysteine motif, all chemokines share the similar spatial topology. Common structural features include a flexible N-terminus, N-loop, single-turn 3_{10}-helix followed by three β-strands and C-terminal α-helix (1). Three β-strands are connected to each other by 30s and 40s loops, while the 50s loop links the C-terminal α-helix to the β_3-strand. Chemokines control cell trafficking by interactions with chemokine G protein-coupled receptors (GPCRs) and endothelial cells glycosaminoglycans (GAGs). Chemokines activate GPCRs through binding of the receptor N-terminus (chemokine recognition site 1, CRS1) and the transmembrane pocket (chemokine recognition site 2, CRS2) via its globular core (the N- and 40s loops) and flexible N-terminus respectively (2–4). Chemokine-receptor interactions are redundant and usually several chemokines can activate one GPCR (5). At the same time low affinity interactions of chemokines with GAGs create haptotactic gradients that direct cell migration (6). Combined with chemokine oligomerization (7) and heterodimerization (8, 9), these interactions form a complex signalling network which regulate immune and inflammatory responses.

Pathogens such as viruses, worms, and ticks target different parts of the chemokine network in order to avoid the host immune response (10–12). Ticks gain particular interest because their saliva contains numerous bioactive compounds, including proteins, and could be a rich source of candidates for drug development (13). Among those bioactive compounds are Evasins, a class of chemokine-binding proteins (CKBPs) first isolated from saliva of the brown dog tick *Rhipicephalus sanguines* (14, 15). Until now the class consist of three family members: Evasin-1, Evasin-3 and Evasin-4. However, several hundreds of proteins distantly related to Evasins have been identified in eight different tick species (16). In general, Evasins can be divided up in two subclasses: C8 fold (Evasin-1, -4) and C6 fold (Evasin-3) containing 8 and 6 cysteines, respectively. Evasin-1 and Evasin-4 show efficient binding to human CC-chemokines, such as CCL5 (RANTES) and CCL3, whereas Evasin-3 show high affinity to CXC-type chemokines, in particular CXCL8 (interleukin-8, IL-8) and CXCL1 (Gro-α).

CXCL8 is an inflammatory chemokine associated with the development of numerous diseases such as neurodegenerative and pulmonary disorders, several types of cancer, psoriasis and rheumatism (17–19). It has been shown that direct targeting of CXCL8 by antibodies has beneficial effects during acute lung injury (20), meconium aspiration syndrome (21), chronic obstructive pulmonary disease (22) and psoriasis (23). Several low-affinity CXCL8-binding peptides and peptidomimetics have been derived from CXCR1/2 chemokine-binding sites and showed activity in both *in vitro* and *in vivo* studies (24, 25). Administration of Evasin-3 has a beneficial effect during myocardial ischemia, which is attributed to its chemokine-binding activity (26). Thus, Evasin-3 could be considered as a promising alternative to antibodies and chemokine-binding peptides, combining high-affinity and easy accessibility by chemical synthesis due to its relatively small size.

In contrast to Evasin-1 (27) and -4 (28), Evasin-3 has not been in the focus of structural research and no structures of Evasin-3 or its complexes with chemokines are available so far. In the present study, we investigated structures of Evasin-3 and CXCL8/Evasin-3 complex using solution NMR spectroscopy. Furthermore, we developed two new high-affinity CXCL8 binding peptides based on the experimentally determined structure of the CXCL8/Evasin-3 complex. Both peptides showed potent anti-inflammatory activity *in vitro*.

Results

Expression of Evasin-3

Expression of recombinant Evasin-3 in *E.coli* yielded two major products with molecular masses of 7,000 and 7,130 Da that corresponded to native Evasin-3 and a variant with a N-terminal methionine (designated as met-Evasin-3), respectively (Fig. S1). Oxidative folding in the presence of the cysteine/cystine redox couple resulted in a 6 Da decrease of the molecular weight for both variants, indicating the loss of 6 protons with formation of three disulfide bonds. The expression level of met-Evasin-3 was substantially higher and for that reason this variant was used for further NMR spectroscopy studies.

NMR analysis of [^{15}N, ^{13}C] met-Evasin-3

Sequential assignment of met-Evasin-3 was carried out by a combination of 2D and triple resonance 3D spectra. Analysis of ^{15}N-^{1}H HSQC spectra at various temperatures and concentrations showed the presence of extensive line broadening of proton signals, which could

only be resolved by recording spectra at elevated temperature (44°C). Under these conditions all expected amide peaks in met-Evasin-3 were observed with the exception of V19 (Fig. S2A). In addition, conformational heterogeneity of certain amide peaks was observed for the S3-R8 and S58-R66 regions that relates to intermolecular aggregation at higher protein concentrations. The met-Evasin-3 secondary structure was first predicted by the CSI 3.0 webserver using available experimental chemical shifts for backbone atoms. According to these chemical shifts met-Evasin-3 consists of three short β-strands in V19-S21, C37-G40, and H49-K52 regions, whereas the rest of the protein is predicted to be in the random coil state (Fig. 1D). Heteronuclear ^{15}N NOE relaxation values were measured in order to determine flexibility disorder of met-Evasin-3. (Fig. 2). Negative values for residues in the N-terminal L1-D15 and C-terminal L57-R66 regions indicated high backbone flexibility whereas the cysteine-rich core S21-Y51 showed positive relaxation values >0.5 corresponding to a relatively rigid structure.

NMR analysis of CXCL8/met-Evasin-3 complex

The complex of [^{15}N, ^{13}C] CXCL8 with unlabeled met-Evasin-3 and the reverse isotope-labeled system was used to study the structure of the CXCL8/met-Evasin-3 complex by NMR spectroscopy. Titration of [^{15}N, ^{13}C] CXCL8 by unlabeled met-Evasin-3 caused changes of chemical shifts of CXCL8 amide atoms, albeit complex formation proceeded relatively slowly at pH 4.5 and final equilibrium was only achieved after incubation up to 1 hour at 37°C (Fig S3). After reaching equilibrium at a molar ratio of 1:1, further addition of met-Evasin-3 did not lead to changes in the ^{15}N-^{1}H HSQC spectrum, indicating 1:1 stoichiometry of the CXCL8/met-Evasin-3 complex. The pattern of met-Evasin-3-induced chemical shift changes of amide atoms in CXCL8 demonstrated that most affected residues were located in the β1-, β2-strand, and the α-helix of CXCL8 (Fig. 1A-B). Significant changes in chemical shifts were also observed for the N-loop (Y13-K15) and the 50s loop (D52-K54).

At NMR concentrations (1 – 500 μM), CXCL8 is present as a dimer. Absence of CXCL8 dimer-specific intermolecular NOE signals, e.g. E29-A69, E29-L25, in the [^{15}N, ^{13}C] CXCL8/met-Evasin-3 complex indicates that binding of met-Evasin-3 caused CXCL8 dimer disruption (Fig. S4). NOE restraints extracted from ^{13}C- and ^{15}N-edited NOESY spectra and TALOS predicted dihedral angles were used to calculate the set of CXCL8 structures in the complex with met-Evasin-3 (Fig. S5A-B). In contrast to the CXCL8 structure in the dimer, the CXCL8 α-helix in the CXCL8/met-Evasin-3 complex is repositioned and oriented almost orthogonally to the β-sheet (Fig. 3A). The region F17-E24 is twisted and pushed away forming the cavity between the CXCL8 N-loop and the α-helix.

Similarly, NMR spectra were recorded for the reverse labeled CXCL8/[^{15}N, ^{13}C] met-Evasin-3 complex. Binding of CXCL8 to met-Evasin-3 drastically decreased line broadening of the most core met-Evasin-3 NMR resonances. The CXCL8-induced chemical shift perturbation pattern of amide peaks is displayed in Fig. 1C-D. Spectral changes were especially high for the T27-Q30 and C38-L41 regions. Heteronuclear NOE relaxation data indicated that binding of CXCL8 increased rigidity of the met-Evasin-3 C-terminal N56-V63 and L42-K47 residues, while the N-terminal part L1-D12 showed even higher flexibility (Fig. 2). Met-Evasin-3 in the complex possessed more defined secondary structure compared to that of the free form (Fig. 1B). All three β-strands were extended upon binding of CXCL8 and two I type turns were also predicted in regions Q30-C33 and Q44-K47. The structure of [^{15}N, ^{13}C] met-Evasin-3 in the CXCL8/[^{15}N, ^{13}C] met-Evasin-3 complex was calculated using integrated NOE peaks and TALOS predicted dihedral angles (Fig. S5C-D). Average RMSD values for backbone atoms in the F17 - N56 region were calculated to be 2.0 Å and we used these structures mainly as an auxiliary tool for further manual NOESY spectra assignment.

Residues involved in complex formation were mapped using ^{15}N and ^{13}C-filtered NOESY experiments on the [^{15}N, ^{13}C] CXCL8/met-Evasin-3 complex. Multiple intermolecular NOE signals were observed between the F38-L42 region of met-Evasin-3 and the L25-I28 region of CXCL8 in both ^{15}N and ^{13}C NOESY spectra (Fig. S6). Strong NOE signals were found between V61 in the CXCL8 α-helix and residues V19, I53, and F38 of met-Evasin-3.

GAGs and met-Evasin-3 competition for [^{15}N, ^{13}C] CXCL8 binding

In order to study competition between Evasin-3 and GAGs for CXCL8 binding, [^{15}N, ^{13}C] CXCL8 was first titrated with increasing concentrations of Dalteparin (Fragmin®, Pfizer) - low molecular weight heparin with the average molecular weight

of 5 kDa. Unfortunately, addition of Fragmin caused intensity losses and significant deterioration of NMR spectra, most likely caused by aggregation. Fondaparinux (Arixtra®, GSK), which comprises the five central sulfated sugar units in heparin, has the well-defined composition and the lower molecular weight (1.7 kDa) comparing with Fragmin. For that reason, Fondaparinux facilitates collection of NMR spectra of higher quality and was chosen for further NMR titration experiments. The highest perturbations by Fondaparinux were observed for residues of the CXCL8 α-helix (W57, R60, R68, E70) and the N-loop (K15, H18, K23) (Fig. S7). Observed changes were consistent with results of previous studies describing the interaction of CXCL8 with several heparin oligosaccharides (29). Addition of met-Evasin-3 to the CXCL8/GAG (at a 1:1 ratio) complex completely abolished GAG binding and peak positions of CXCL8 slowly reverted back corresponding to the CXCL8/met-Evasin-3 complex, even in the case of ten-fold excess of Fondaparinux (Fig. S8).

Size exclusion chromatography of CXCL8/met-Evasin-3 complex

To support findings from previous NMR experiments, CXCL8/met-Evasin-3 complex formation was assessed by size-exclusion chromatography. CXCL8 at a concentration of 0.1 mg/ml eluted into a single unsymmetrical peak that corresponded to the molecular weight of dimeric CXCL8 (Fig. S9A). Addition of met-Evasin-3 at a concentration of 0.1 mg/ml caused no immediate changes, however after 1-hour incubation at 37°C the peak shifted to a higher molecular weight of 17 kDa. When obligatory monomeric V27P/E29P CXCL8 (30) was used in the similar experiment, the peak moved immediately from 8 kDa to 17 kDa, indicating significantly faster kinetics of the complex formation (Fig. S9B). Observed higher molecular weights of met-Evasin-3 and CXCL8/met-Evasin-3 complex were probably caused by met-Evasin-3 unstructured termini, which would increase the hydrodynamic radius of both free Evasin-3 and the CXCL8/met-Evasin-3 complex. The mixture of 1 mg/ml low molecular weight heparin (Fragmin®) and 0.1 mg/ml of CXCL8 eluted as a single broad peak, indicating formation of the CXCL8/GAG complex with a molecular weight of 35 kDa (Fig. 4). When met-Evasin-3 was added to this CXCL8/GAG complex, the mixture eluted as two separate peaks with molecular weights of 35 and 10 kDa, whereas only the peak corresponding to 17 kDa was observed after 1-hour incubation at 37°C.

Truncated Evasin-3 (tEv3 17-56)

To study the relative importance of the flexible unstructured N- and C-terminus of met-Evasin-3 on binding CXCL8, L1-N16 and L57-R66 regions were removed, leading to a truncated Evasin-3 variant, designated as tEv3 17-56 (31). Truncation resulted in largely diminished broadening ^{1}H NMR resonances, gaining a higher number of NOE peaks necessary for calculation of a better resolved structure. In addition, TALOS predicted dihedral angles and experimentally assigned disulfide bonds (31) were used to obtain the final high resolution structure of tEv3 17-56 (Fig. 3B). tEv3 17-56 adopts an L-shaped structure. The short arm of the L is formed by two loops T27-E32 and G40-D49, connected together by the P34-F38 loop. In contrast to the rigid T27-E32 loop, the tip of the G40-D49 loop, formed by residues L42-N45, is more flexible. Loops are arranged by six cysteines linked into the disulfide pattern where the C26-C39 disulfide bond protrudes through the ring formed by the C22-C37 and C33-C50 disulfides. The flanking D18-S21 and H49-I54 regions constitute two short beta-strands and form the long arm of the L-shaped structure.

tEv3 17-56 tightly binds CXCL8 at a 1:1 stoichiometry and results in a similar pattern of CXCL8 chemical shifts backbone perturbations as was observed for full-length met-Evasin-3 (Fig. S10). Only K20 and K64 residues of CXCL8 do not follow the same tendency and showed substantial difference compared to the met-Evasin-3-induced pattern. Taking into account that tEv3 17-56 binds CXCL8 in the same way as full length met-Evasin-3, the model of CXCL8/tEv3 17-56 complex was calculated using HADDOCK. Calculated structures of CXCL8 in the CXCL8/met-Evasin-3 complex and tEv3 17-56 were used as a starting point for calculation and combined with experimentally observed NOE contacts in the CXCL8/met-Evasin-3 complex. tEv3 17-56 N- and C-termini fitted into the cavity between the α-helix and the F17-E24 loop, while the G40-D49 loop binds to the β1-strand of CXCL8 (Fig 3C, Table S1). According to the low-energy models, both tEv3 17-56 N- and C-termini were located in proximity of K20 and K64 of CXCL8 that could explain the difference in the chemical shift of these CXCL8 residues.

Truncated cyclic Evasin-3

The formation of a beta-sheet by the spatially close N- and C-terminus of tEv3 17-56 provides an opportunity to cyclize the peptide via the backbone. In previous studies it has been shown that beta-hairpins capped with a β-turn D-Pro-Gly motif stabilizes short loops (32). To introduce this β-turn into tEv3 17-56, an additional N-terminal residue from the Evasin-3 sequence was added to the sequence to match the length of N- and C-terminal regions. The resulting sequence containing the Evasin-3 region N16-N56 and the D-Pro-Gly sequence was synthesized by Boc-SPPS and cyclized using intermolecular native chemical ligation. Subsequent oxidative folding resulted in truncated cyclic Evasin-3 16-56 with a D-Pro-Gly turn (designated as tcEv3 16-56 dPG) (Fig. 5A).

Affinity of Evasin-3 variants

Affinity of Evasin-3 and its variants to CXCL8 was studied by SPR biosensor analysis using C-terminally biotinylated CXCL8 immobilized on a streptavidin modified chip surface. Evasin-3 variants bound CXCL8 in a dose-dependent manner. Native Evasin-3 showed slower association and dissociation kinetics compared to truncated variants (Fig. 5B, S11). At higher Evasin-3 concentrations, no increase in RU signal and curvature were observed in the SPR sensorgrams, restricting further affinity analysis. Saturated binding analysis for truncated variants resulted in Kd values of 27 nM and 13 nM for tEv3 17-56 and tcEv3 16-56 dPG, respectively.

Plasma stability

Proteolytic stability of full-length Evasin-3 and its variants was tested in pooled human plasma from healthy volunteers (Fig. S12A). After 2 hours of incubation at 37°C in human plasma full-length Evasin-3 degraded nearly quantitatively, losing C-terminal R66 and R65 (ΔC_1 and ΔC_2 respectively). Moreover, after 18 hours of incubation only ΔC_2 could be detected in solution. In contrast to the full-length protein, the truncated Evasin-3 variants showed no detectable signs of degradation after 18 hours of incubation in human plasma (Fig. 5C, S12B).

PMN migration assay

In order to assess the anti-CXCL8 activity of Evasin-3 variants, polymorphonuclear neutrophils (PMN) migration assays were performed. Addition of 1 nM CXCL8 induced significant migration of PMNs (624 ± 458 PMN/mm^2) compared with controls (98 ± 83 PMN/mm^2) in absence of chemoattractant (Fig. 6). Migration was inhibited by addition of 10 nM of Evasin-3 (206 ± 203 PMN/mm^2). Significant effects were observed in the presence of tEv3 17-56 (223 ± 189 PMN/mm^2) and tcEv3 16-56 dPG (160 ± 65 PMN/mm^2).

Identification of Evasin-3 homologues.

A search against UniProtKB using the BLASTp server yielded 35 protein sequences with 69% - 39% sequence identity. Of these 15 were identified to come from *Ixodes* genus, 12 – from *Rhipicephalus*, 7 – from *Amblyomma*, and one from *Hyalomma*. In all cases, six cysteine positions were conserved, while hydrophobic residues in regions preceding C1 and following C5 and C6 residues (Fig. S13) appeared invariant.

Discussion

Evasins are a family of tick salivary chemokine-binding proteins comprised of two subfamilies. Whereas Evasin-1 and -4 comprise 8 cysteines, Evasin-3 contains 6 cysteines located in the compact core region. The three-dimensional structure of the Evasin-3 core is largely determined by its three disulfide bonds. The C26-C39 bond protrudes through the ring comprised by the C22-C37 and C33-C50 forming an inhibitory cystine-knot (ICK) motif. Although the core sequence of Evasin-3 fits the consensus sequence for the ICK motif having five loops that are separated by conserved cysteines (33), no structural homology to known proteins could be found in DALI or in the Knottin3D database. The scaffold of Evasin-3 is predominantly composed by T27-E32 and G40-H49 loops. The T27-E32 loop is rigid, whereas the G40-H49 loop is relatively flexible. Since Evasin-3 binds closely related CXCL1 and CXCL8 chemokines and G40-H49 loop composes the great part of CXCL8/Evasin-3 complex interface, flexibility of this region could be necessary to fine-tune the spatial structure of the binding region during complex formation with different targets. The ICK motif is common for conotoxins (34), spider venoms and cyclotides (35), but examples among tick proteins are rare and to our knowledge are limited to holocyclotoxins (36, 37). Database search identified 35 putative Evasin-3 homologues which share inhibitory cystine knot motif. Identified sequences embodies conservative regions of hydrophobic residues which compose the complex interface in the case of CXCL8/Evasin-3 complex. That most likely indicates a similar chemokine binding mode for these putative Evasins.

In contrast to Evasin-1, where both the N- and C-terminus play a crucial role in chemokine binding (27, 38), neither N- nor C-terminus of Evasin-3 participate in CXCL8 binding. Moreover, N- and C-terminus are predicted to be highly glycosylated (Fig. 1C), which is consistent with earlier observation that glycosylation of Evasin-3 does not play an essential role in chemokine binding (14). To study the effect of termini on binding, we synthesized two novel CXCL8 binding peptides – linear tEv3 17-56 and cyclic tcEv3 16-56 dPG, both retaining the ICK bundled core of the native protein. The ICK motif is known to contribute drastically to increase of protein and peptide stability under harsh extracellular conditions (39). The equally high proteolytic stability of the linear tEv3 17-56 and cyclic tcEv3 16-56 dPG in human plasma is in accordance with previous studies indicating that presence of a cystine knot is more vital for peptide stability than a cyclized backbone (40, 41). Although both tEv3 17-56 and cyclic tcEv3 16-56 dPG keep nM-affinity to CXCL8 (Kd values of 27 and 13 nM, respectively), these Kd values fall significantly above the 0.43 nM Kd value previously measured for native Evasin-3 (14). Apparently, the presence of long N- and C-termini has a direct effect on internal dynamics of Evasin-3 structure that causes slower association and dissociation rates of binding CXCL8 and thus lower Kd values.

Final energy-minimized models of the complex between CXCL8 and tEv3 17-56 were calculated by HADDOCK using experimentally observed CXCL8/met-Evasin-3 contacts. It has been shown that Evasin-1 and Evasin-4 binding to chemokine N-terminal regions prevent their interactions with chemokine-receptor recognition site 2 (27, 28). Evasin-3 leaves both receptor-binding sites of CXCL8 unoccupied and available for possible alternative interactions (42–45). To test this hypothesis PMN migration assays were performed. CXCL8 acted as a potent chemoattractant through interaction with its cognate CXCR1/2 receptors. However, the present data showed that CXCL8 bound to Evasin-3, or one of the truncated variants, was unable to induce PMN migration and thus activate the CXCR2 receptor presented on the cell surface. This observation could be explained by structural changes in the N-loop of CXCL8, which residues are crucial for binding of the CXCR1/2 N-domain (46). Although Evasin-3 does not directly interact with the receptor binding region of CXCL8 N-loop, significant perturbations were observed for Y13-F17 residues upon binding of Evasin-3 and the truncated variant tEv3 17-56. These perturbations were most likely caused by internal changes in CXCL8 packing upon formation of the complex. Indeed, Evasin-3 binding caused substantial repositioning of the α-helix and the N-loop comparing with CXCL8 dimer and physiologically active obligatory CXCL8 monomers (42, 47).

According to the obtained model, the C39-Q44 core region of Evasin-3 binds the CXCL8 β1-strand and the C-terminal helix, thereby partially blocking the CXCL8 dimer interface. Although Evasin-3 quickly binds to monomeric V27P/E29P CXCL8, SEC and NMR experiments showed that binding to native CXCL8 dimer is kinetically slow. That could indicate that the rate-limiting step in the CXCL8/Evasin-3 complex formation is the CXCL8 dimer dissociation and the primary target of Evasin-3 is the CXCL8 monomer present in the blood stream. This also means that influence of the chemokine oligomeric state should be taken into account during the assay design for research on chemokine-binding proteins that enables a more comprehensive view on chemokine/chemokine-binding protein relationships.

GAGs are believed to be a storage for CXCL8 and orchestrate levels of free dimeric and monomeric CXCL8 (48). CXCL8 binding to GAGs is mediated through interactions with positively charged residues in the N-loop and the C-terminal α-helix of CXCL8 (29, 49). Flanking β-strands of Evasin-3 intercalate between the CXCL8 α-helix and the N-loop, preventing binding of CXCL8 to GAGs by disrupting the continuous stretch of positively charged residues of the CXCL8 GAG-binding site. Both NMR and SEC experiments showed that Evasin-3 can compete with GAG-binding and slowly substitute GAGs from the CXCL8/GAGs complex. The rate-limiting step in this substitution apparently is release of monomeric CXCL8. As a result, Evasin-3 not only neutralizes active monomeric CXCL8 in the blood stream but also depletes the storage of CXCL8 in the GAG-bound form.

In summary, 3D structures of Evasin-3 and its complex with chemokine CXCL8 have been studied by solution NMR spectroscopy. Evasin-3 represents a rare example of a tick protein with an inhibitory cysteine knot motif. Tight binding of Evasin-3 to the CXCL8 monomer blocks interactions with CXCR2 and disrupts the GAG binding interface, leading to elimination of both chemotactic and haptotactic gradients. Two novel

CXCL8 binding peptides were derived from the Evasin-3 sequence – linear tEv3 17-56 and cyclic tcEv3 16-56 dPG. These short variants are easily accessible by chemical synthesis combining high affinity to CXCL8 with great proteolytic stability. Importantly, synthetic Evasin-3 variants can be used as a scaffold for design and fine-tuning of new selective chemokine-binding agents.

Experimental procedures

Expression of recombinant proteins. The pET23a vector containing human CXCL8 (UniProt: p10145, 6-77) and monomeric variant V27P/E29P CXCL8 and pET30a containing Evasin-3 (UniProt: p0c8e8, 1-66) genes were purchased from GenScript, USA. Both proteins were expressed in BL21 (DE3) Star (Novagen). Cells were grown in 1L standard LB media at 37°C in the presence of the required antibiotic. Once the OD_{600} value reached 0.6-0.8, expression of protein was induced with 0.1 mM or 1 mM of isopropyl β-D-1-thiogalactopyranoside IPTG (Sigma-Aldrich) in the case of pET23a and pET30a vector respectively. Cells were harvested 3 hours after induction by centrifugation at 4,000 rpm for 20 min at 4°C.

In order to obtain [^{15}N, ^{13}C]-labeled proteins, cells were grown in LB media as described above. After OD_{600} reached 0.6-0.8, cells were harvested by centrifugation at 4,000 rpm at 4°C and transferred to M9 media. Prior to induction with IPTG, cells were incubated in media for 1 hour to deplete internal carbon and nitrogen sources. At induction, media was supplemented with 1g/L of ^{13}C-glucose and $^{15}NH_4Cl$, incubated for 3 hours and harvested by centrifugation.

Cells were re-suspended in 50 mM Tris pH 8 and lysed with 1x Bugbuster (Novagen) and 0.1 U/ml benzonaze® nuclease (Sigma-Aldrich). For CXCL8, cells were lysed and the supernatant was discarded by centrifugation at 10,000 rpm for 20 min at 4°C. Insoluble fraction was washed twice with 50 mM Tris pH 8 and once with 50 mM Tris pH 8, 0.5% Tween-20. Insoluble pellets were dissolved in, 0.1 mM Tris pH 8, 200 mM DTT, 6 M Gdn-HCl and dialyzed overnight against 0.5% acetic acid using a 3.5 kDa Spectra/Por RC membrane (Repligen). In the case of Evasin-3, cell debris was removed by centrifugation at 10,000 rpm for 20 min at 4°C, and the soluble fraction was dialyzed as described above. The soluble fractions after dialysis were centrifuged at 10,000 rpm for 20 min at 4°C and then lyophilized.

Lyophilized material was dissolved in 6 M Gdn-HCl, 0.1 mM Tris pH 8 at 20 mg/ml and then added dropwise to 1 M Gdn-HCl, 0.1 mM Tris pH 8, 10 mM cysteine, 1 mM cystine, at 4°C to a final concentration of 1 mg/ml. Folded proteins were purified by HPLC using 22mm x 250mm Vydac C18 columns, analyzed by LC-MS and lyophilized.

Peptide synthesis. tEv3 17-56 and tcEv3 16-56 dPG were synthesized by Boc-SPPS and folded as described previously (31). For one-pot intramolecular cyclization and folding, crude tcEv3 16-56 dPG was dissolved at a concentration of 0.2 mg/ml in 50 mM ammonium bicarbonate buffer pH 8. After completion of the reaction the folded cyclic peptide was purified by HPLC and lyophilized.

Surface Plasmon Resonance. Affinity assays of Evasin-3 variants were performed using BIAcore T200 surface plasmon resonance system (GE Healthcare, Sweden). All assays were carried out in PBS buffer pH 7.4, supplemented with 0.05% Tween-20 as running buffer. 70 RU of chemically synthetized CXCL8-Biotin was immobilized on a SAHC 200M sensorchip (Xantec, Germany) according to the manufacturer's protocol. Concentration series of Evasin-3 variants, ranging from 1 µM to 2 nM, were prepared by 2-fold dilution of 50 µM stock solutions. Association and dissociation kinetics were monitored at flow rate 30 µl/min for 250 s and 300 s, respectively. Data were analyzed using BIAcore T200 software and BIAEvaluation software (GE Healthcare, Sweden) using a steady-state affinity equation with a linear component.

NMR.

NMR samples were prepared from freeze-dried proteins as 0.2 mM solutions in 25 mM deuterated NaAc-d^3 buffer pH 4.5 containing 0.1 mM EDTA, 0.2 mM sodium azide and 5% (v/v) D_2O for deuterium lock. To remove TFA salts presented in freeze-dried samples of proteins, initial buffer exchange was carried out by ultracentrifugation (in 4-5 steps) using pre-washed Amicon Ultra-3000 3 kDa (Millipore, USA) ultracentrifugation filters. Final NMR solutions were prepared in Wildman 3 mm NMR tubes (160 µl volume), containing traces of DSS for internal chemical shift calibration (0 ppm ^{1}H). All NMR spectra were recorded using Bruker Avance III HD 700 MHz spectrometer, equipped with a cryogenically cooled TCI probe. Sample

temperature was set to 25, 37 or 44°C, with the accurate probe temperature calibrated using a thermocouple inside an NMR tube that was inserted into the probe. Backbone resonance assignment of met-Evasin-3, tEv3 17-56 and CXCL8 was derived from a combination of ^{15}N-^{1}H HSQC, HNCO, HNCACO, HNCACB and CBCA(CO)NH spectra. Aliphatic side chain resonances were assigned using ^{13}C-^{1}H HSQC and hCCH DIPSI spectra. Distance constraints were extracted from ^{15}N and ^{13}C NOESY spectra.

To study the Evasin-3/CXCL8 1:1 complex, two different samples were prepared with either [^{15}N, ^{13}C] met-Evasin-3 or [^{15}N, ^{13}C] CXCL8 as labelled component at the final concentration 200 µM. Titrated complexes contain a slight excess of unlabeled CXCL8 or met-Evasin-3, respectively. After completion of complex formation, a set of triple resonance spectra spectra, as described above, were recorded for both met-Evasin-3 and CXCL8 in the bound form. Intramolecular contacts of CXCL8 and met-Evasin-3 were obtained from filtered ^{15}N and ^{13}C NOESY experiments.

For GAGs bindings experiments low-molecular weight heparin Delteparin (commercial name Fragmin®, Pfizer) and Fondaparinux (commercial name Arixtra®, GSK) were purchased from a pharmacy as solutions for injections. 25 µM of [^{15}N, ^{13}C] CXCL8 was titrated by increasing concentration of aliquots from a stock solution of 5 mg/ml Fondaparinux or Fragmin to the final GAG concentration of 0.2 mM at 25°C, pH 7.1. In the next step, 30 µM of met-Evasin-3 was added to the solution to monitor the displacement of bound Fondaparinux and follow Evasin-3 / CXCL8 complex formation by a series of 1D proton and ^{15}N-^{1}H HSQC spectra.

Spectra processing was performed by Bruker Topspin 3.2 and Sparky 3.114 software. The secondary structure was predicted by CSI 3.0 webserver (50). Structure calculations were performed by dynamics simulated annealing method using Xplor-NIH software (51, 52) and refined via the NMRe web server (53). Structure refinement of the complex was performed using HADDOCK 2.2 server (54).

Size exclusion chromatography. SEC experiments were carried out on a Varian ProStar 215 solvent delivery system, coupled to a Varian ProStar 320 UV/VIS detector set at a wavelength of 280 nm. Separation was performed using a BioSep 5 um SEC-s2000 145Å, 300 x 4.6 mm LC column (Phenomenex, Torrance, CA, USA). 50 mM sodium phosphate buffer pH 6.65 containing 150 mM NaCl was used as eluent buffer. Flow rate was set at 0.5 ml/min. Proteins were injected at 0.1 mg/ml concentration in the presence or absence of 1 mg/ml low molecular weight heparin (commercial name Fragmin®, Pfizer). Molecular weights of proteins were calculated using the calibration curve provided by the manufacturer.

Plasma stability. 100 µg of Evasin-3 variants were dissolved in 100 µl of normal plasma taken from a healthy volunteer and incubated at 37°C. At a required timepoint reaction was stopped by addition of 15 µl of 20% TCA to 15 µl aliquot of a sample and analyzed by LC-MS.

Bioinformatics. Glycosylation sites were predicted using NetNGlyc 1.0 and NetOGlyc 4.0 servers. The threshold for both positive N- and O-glycosylation sites was set at 0.5.

For homology search, Evasin-3 sequence (UniProt ID: p0c8e8) was used as a query for BLASTp algorithm against UniProtKB database (55). Multiple sequence alignment was performed using Clustal Omega algorithm (56) with default settings and results were visualized by JalView 2.10 software.

PMN isolation and migration. Human neutrophils were isolated from the blood of healthy donors as described previously (57). Isolated neutrophils were resuspended at (10^6 cells/mL) in RPMI 1640 medium supplemented with 1% fetal calf serum. A 12-well chemotaxis chamber with a 5 µm polycarbonate membrane (Neuroprobe, Gaithersburg, MD) was used to assess the migration of neutrophils towards the chemoattractant CXCL8 (1 nM) in presence or absence of Evasin-3 variants (10 nM). The chemoattractant was added in the lower wells and the neutrophils ($1x10^5$ cells) were seeded in the upper wells. After incubation of 90 min at 37°C, the non-migrated cells were carefully removed and the membrane was stained with Diff-Quick stain (Eberhard Lehmann GmbH, Berlin, Germany). Migrated cells were visualized by light microscopy, counted manually in three fields of view and expressed as cells/mm^2. Data were analysed by GraphPad Prism 8.0 software using one-way ANOVA statistical test.

Conflict of interest: The authors declare that they have no conflicts of interest with the contents of this article.

References

1. Fernandez, E. J., and Lolis, E. (2002) Structure, Function, and Inhibition of Chemokines. *Annu. Rev. Pharmacol. Toxicol.* **42**, 469–499
2. Zheng, Y., Han, G. W., Abagyan, R., Wu, B., Stevens, R. C., Cherezov, V., Kufareva, I., and Handel, T. M. (2017) Structure of CC Chemokine Receptor 5 with a Potent Chemokine Antagonist Reveals Mechanisms of Chemokine Recognition and Molecular Mimicry by HIV. *Immunity*. **46**, 1005–1017.e5
3. Burg, J. S., Ingram, J. R., Venkatakrishnan, A. J., Jude, K. M., Dukkipati, A., Feinberg, E. N., Angelini, A., Waghray, D., Dror, R. O., Ploegh, H. L., and Garcia, K. C. (2015) Structural biology. Structural basis for chemokine recognition and activation of a viral G protein-coupled receptor. *Science*. **347**, 1113–7
4. Qin, L., Kufareva, I., Holden, L. G., Wang, C., Zheng, Y., Zhao, C., Fenalti, G., Wu, H., Han, G. W., Cherezov, V., Abagyan, R., Stevens, R. C., and Handel, T. M. (2015) Structural biology. Crystal structure of the chemokine receptor CXCR4 in complex with a viral chemokine. *Science*. **347**, 1117–22
5. Hughes, C. E., and Nibbs, R. J. B. (2018) A guide to chemokines and their receptors. *FEBS J.* **285**, 2944–2971
6. Proudfoot, A., Johnson, Z., Bonvin, P., and Handel, T. (2017) Glycosaminoglycan Interactions with Chemokines Add Complexity to a Complex System. *Pharmaceuticals*. **10**, 70
7. Wang, X., Sharp, J. S., Handel, T. M., and Prestegard, J. H. (2013) Chemokine Oligomerization in Cell Signaling and Migration. in *Progress in Molecular Biology and Translational Science*, pp. 531–578, **117**, 531–578
8. Weber, C., and Koenen, R. R. (2006) Fine-tuning leukocyte responses: towards a chemokine "interactome". *Trends Immunol.* **27**, 268–73
9. von Hundelshausen, P., Agten, S. M., Eckardt, V., Blanchet, X., Schmitt, M. M., Ippel, H., Neideck, C., Bidzhekov, K., Leberzammer, J., Wichapong, K., Faussner, A., Drechsler, M., Grommes, J., van Geffen, J. P., Li, H., Ortega-Gomez, A., Megens, R. T. A., Naumann, R., Dijkgraaf, I., Nicolaes, G. A. F., Döring, Y., Soehnlein, O., Lutgens, E., Heemskerk, J. W. M., Koenen, R. R., Mayo, K. H., Hackeng, T. M., and Weber, C. (2017) Chemokine interactome mapping enables tailored intervention in acute and chronic inflammation. *Sci. Transl. Med.* **9**, eaah6650
10. Proudfoot, A. E. I., Bonvin, P., and Power, C. A. (2015) Targeting chemokines: Pathogens can, why can't we? *Cytokine*. **74**, 259–267
11. Heidarieh, H., Hernáez, B., and Alcamí, A. (2015) Immune modulation by virus-encoded secreted chemokine binding proteins. *Virus Res.* **209**, 67–75
12. González-Motos, V., Kropp, K. A., and Viejo-Borbolla, A. (2016) Chemokine binding proteins: An immunomodulatory strategy going viral. *Cytokine Growth Factor Rev.* **30**, 71–80
13. Kazimírová, M., and Štibrániová, I. (2013) Tick salivary compounds: their role in modulation of host defences and pathogen transmission. *Front. Cell. Infect. Microbiol.* **3**, 43
14. Déruaz, M., Frauenschuh, A., Alessandri, A. L., Dias, J. M., Coelho, F. M., Russo, R. C., Ferreira, B. R., Graham, G. J., Shaw, J. P., Wells, T. N. C., Teixeira, M. M., Power, C. a, and Proudfoot, A. E. I. (2008) Ticks produce highly selective chemokine binding proteins with antiinflammatory activity. *J. Exp. Med.* **205**, 2019–31
15. Déruaz, M., Bonvin, P., Severin, I. C., Johnson, Z., Krohn, S., Power, C. a., and Proudfoot, A. E. I. (2013) Evasin-4, a tick-derived chemokine-binding protein with broad selectivity can be modified for use in preclinical disease models. *FEBS J.* **280**, 4876–4887
16. Singh, K., Davies, G., Alenazi, Y., Eaton, J. R. O., Kawamura, A., and Bhattacharya, S. (2017) Yeast surface display identifies a family of evasins from ticks with novel polyvalent CC chemokine-binding activities. *Sci. Rep.* **7**, 4267
17. Ning, Y., and Lenz, H. (2012) Targeting IL-8 in colorectal cancer. *Expert Opin. Ther. Targets*. **16**, 491–497
18. Mamik, M. K., and Ghorpade, A. (2016) CXCL8 as a Potential Therapeutic Target for HIV-Associated Neurocognitive Disorders. *Curr Drug Targets*. **17**, 111–121
19. Ha, H., Debnath, B., and Neamati, N. (2017) Role of the CXCL8-CXCR1/2 Axis in Cancer

and Inflammatory Diseases. *Theranostics*. **7**, 1543–1588
20. Bao, Z., Ye, Q., Gong, W., Xiang, Y., and Wan, H. (2010) Humanized monoclonal antibody against the chemokine CXCL-8 (IL-8) effectively prevents acute lung injury. *Int. Immunopharmacol.* **10**, 259–263
21. Mikolka, P., Kopincova, J., Kosutova, P., Kolomaznik, M., Calkovska, A., and Mokra, D. (2018) Anti-IL-8 antibody potentiates the effect of exogenous surfactant in respiratory failure caused by meconium aspiration. *Exp. Lung Res.* **44**, 40–50
22. Mahler, D. A., Huang, S., Tabrizi, M., and Bell, G. M. (2004) Efficacy and Safety of a Monoclonal Antibody Recognizing Interleukin-8 in COPD. *Chest*. **126**, 926–934
23. Tsai, Y.-C., and Tsai, T.-F. (2017) Anti-interleukin and interleukin therapies for psoriasis: current evidence and clinical usefulness. *Ther. Adv. Musculoskelet. Dis.* **9**, 277–294
24. Tanaka, K., Miura, T., Umezawa, N., Urano, Y., Kikuchi, K., Higuchi, T., and Nagano, T. (2001) Rational Design of Fluorescein-Based Fluorescence Probes. Mechanism-Based Design of a Maximum Fluorescence Probe for Singlet Oxygen. *J. Am. Chem. Soc.* **123**, 2530–2536
25. Ezerzer, C., Dolgin, M., Skovorodnikova, J., and Harris, N. (2009) Chemokine receptor-derived peptides as multi-target drug leads for the treatment of inflammatory diseases. *Peptides*. **30**, 1296–1305
26. Montecucco, F., Lenglet, S., Braunersreuther, V., Pelli, G., Pellieux, C., Montessuit, C., Lerch, R., Deruaz, M., Proudfoot, A. E., and Mach, F. (2010) Single administration of the CXC chemokine-binding protein Evasin-3 during ischemia prevents myocardial reperfusion injury in mice. *Arterioscler. Thromb. Vasc. Biol.* **30**, 1371–7
27. Dias, J. M., Losberger, C., Déruaz, M., Power, C. A., Proudfoot, A. E. I., and Shaw, J. P. (2009) Structural basis of chemokine sequestration by a tick chemokine binding protein: the crystal structure of the complex between Evasin-1 and CCL3. *PLoS One*. **4**, e8514
28. Bonvin, P., Dunn, S. M., Rousseau, F., Dyer, D. P., Shaw, J., Power, C. a., Handel, T. M., and Proudfoot, a. E. I. (2014) Identification of the Pharmacophore of the CC Chemokine-binding Proteins Evasin-1 and -4 Using Phage Display. *J. Biol. Chem.* **289**, 31846–31855
29. Joseph, P. R. B., Mosier, P. D., Desai, U. R., and Rajarathnam, K. (2015) Solution NMR characterization of chemokine CXCL8/IL-8 monomer and dimer binding to glycosaminoglycans: structural plasticity mediates differential binding interactions. *Biochem. J.* **472**, 121–133
30. Joseph, P. R. B., Poluri, K. M., Gangavarapu, P., Rajagopalan, L., Raghuwanshi, S., Richardson, R. M., Garofalo, R. P., and Rajarathnam, K. (2013) Proline substitution of dimer interface β-strand residues as a strategy for the design of functional monomeric proteins. *Biophys. J.* **105**, 1491–501
31. Denisov, S. S., Ippel, J. H., Mans, B. J., Dijkgraaf, I., and Hackeng, T. M. (2019) SecScan: a general approach for mapping disulfide bonds in synthetic and recombinant peptides and proteins. *Chem. Commun. (Camb).* **55**, 1374–1377
32. Espinosa, J. F., and Gellman, S. H. (2000) A Designedβ-Hairpin Containing a Natural Hydrophobic Cluster. *Angew. Chemie Int. Ed.* **39**, 2330–2333
33. Craik, D. J., Daly, N. L., and Waine, C. (2001) The cystine knot motif in toxins and implications for drug design. *Toxicon*. **39**, 43–60
34. Miles, L. A., Dy, C. Y., Nielsen, J., Barnham, K. J., Hinds, M. G., Olivera, B. M., Bulaj, G., and Norton, R. S. (2002) Structure of a novel P-superfamily spasmodic conotoxin reveals an inhibitory cystine knot motif. *J. Biol. Chem.* **277**, 43033–43040
35. Rosengren, K. J., Daly, N. L., Plan, M. R., Waine, C., and Craik, D. J. (2003) Twists, knots, and rings in proteins: Structural definition of the cyclotide framework. *J. Biol. Chem.* **278**, 8606–8616
36. Vink, S., Daly, N. L., Steen, N., Craik, D. J., and Alewood, P. F. (2014) Holocyclotoxin-1, a cystine knot toxin from Ixodes holocyclus. *Toxicon*. **90**, 308–317
37. Chand, K. K., Lee, K. M., Lavidis, N. A., Rodriguez-Valle, M., Ijaz, H., Koehbach, J., Clark, R. J., Lew-Tabor, A., and Noakes, P. G. (2016) Tick holocyclotoxins trigger host paralysis by presynaptic inhibition. *Sci. Rep.* **6**, 29446
38. Eaton, J. R. O., Alenazi, Y., Singh, K., Davies, G., Geis-Asteggiante, L., Kessler, B., Robinson, C. V, Kawamura, A., and Bhattacharya, S. (2018) The N-terminal domain of a tick

evasin is critical for chemokine binding and neutralization and confers specific binding activity to other evasins. *J. Biol. Chem.* **293**, 6134–6146
39. Herzig, V., and King, G. F. (2015) The Cystine Knot Is Responsible for the Exceptional Stability of the Insecticidal Spider Toxin ω-Hexatoxin-Hv1a. *Toxins (Basel).* **7**, 4366–80
40. Akcan, M., Clark, R. J., Daly, N. L., Conibear, A. C., De Faoite, A., Heghinian, M. D., Sahil, T., Adams, D. J., Marí, F., and Craik, D. J. (2015) Transforming conotoxins into cyclotides: Backbone cyclization of P-superfamily conotoxins. *Biopolymers*. **104**, 682–692
41. Colgrave, M. L., and Craik, D. J. (2004) Thermal, chemical, and enzymatic stability of the cyclotide kalata B1: the importance of the cyclic cystine knot. *Biochemistry*. **43**, 5965–75
42. Berkamp, S., Park, S. H., De Angelis, A. A., Marassi, F. M., and Opella, S. J. (2017) Structure of monomeric Interleukin-8 and its interactions with the N-terminal Binding Site-I of CXCR1 by solution NMR spectroscopy. *J. Biomol. NMR*. **69**, 111–121
43. Park, S. H., Casagrande, F., Cho, L., Albrecht, L., and Opella, S. J. (2011) Interactions of interleukin-8 with the human chemokine receptor CXCR1 in phospholipid bilayers by NMR spectroscopy. *J. Mol. Biol.* **414**, 194–203
44. Rajagopalan, L., and Rajarathnam, K. (2004) Ligand selectivity and affinity of chemokine receptor CXCR1: Role of N-terminal domain. *J. Biol. Chem.* **279**, 30000–30008
45. Skelton, N. J., Quan, C., Reilly, D., and Lowman, H. (1999) Structure of a CXC chemokine-receptor fragment in complex with interleukin-8. *Structure*. **7**, 157–168
46. Ravindran, A., Joseph, P. R. B., and Rajarathnam, K. (2009) Structural basis for differential binding of the interleukin-8 monomer and dimer to the CXCR1 N-domain: Role of coupled interactions and dynamics. *Biochemistry*. **48**, 8795–8805
47. Rajarathnam, K., Clark-Lewis, I., and Sykes, B. D. (1995) 1H NMR solution structure of an active monomeric interleukin-8. *Biochemistry*. **34**, 12983–12990
48. Joseph, P. R. B., Sawant, K. V., and Rajarathnam, K. (2017) Heparin-bound chemokine CXCL8 monomer and dimer are impaired for CXCR1 and CXCR2 activation: Implications for gradients and neutrophil trafficking. *Open Biol.* 10.1098/rsob.170168
49. Pichert, A., Samsonov, S. a., Theisgen, S., Thomas, L., Baumann, L., Schiller, J., Beck-Sickinger, A. G., Huster, D., and Pisabarro, M. T. (2012) Characterization of the interaction of interleukin-8 with hyaluronan, chondroitin sulfate, dermatan sulfate and their sulfated derivatives by spectroscopy and molecular modeling. *Glycobiology*. **22**, 134–145
50. Hafsa, N. E., Arndt, D., and Wishart, D. S. (2015) CSI 3.0: A web server for identifying secondary and super-secondary structure in proteins using NMR chemical shifts. *Nucleic Acids Res.* **43**, W370–W377
51. Schwieters, C., Kuszewski, J., and Marius Clore, G. (2006) Using Xplor–NIH for NMR molecular structure determination. *Prog. Nucl. Magn. Reson. Spectrosc.* **48**, 47–62
52. Schwieters, C. D., Kuszewski, J. J., Tjandra, N., and Clore, G. M. (2003) The Xplor-NIH NMR molecular structure determination package. *J. Magn. Reson.* **160**, 65–73
53. Ryu, H., Lim, G., Sung, B. H., and Lee, J. (2016) NMRe: a web server for NMR protein structure refinement with high-quality structure validation scores. *Bioinformatics*. **32**, 611–613
54. van Zundert, G. C. P., Rodrigues, J. P. G. L. M., Trellet, M., Schmitz, C., Kastritis, P. L., Karaca, E., Melquiond, A. S. J., van Dijk, M., de Vries, S. J., and Bonvin, A. M. J. J. (2016) The HADDOCK2.2 Web Server: User-Friendly Integrative Modeling of Biomolecular Complexes. *J. Mol. Biol.* **428**, 720–725
55. Bateman, A. (2019) UniProt: a worldwide hub of protein knowledge. *Nucleic Acids Res.* **47**, D506–D515
56. Madeira, F., Park, Y. M., Lee, J., Buso, N., Gur, T., Madhusoodanan, N., Basutkar, P., Tivey, A. R. N., Potter, S. C., Finn, R. D., and Lopez, R. (2019) The EMBL-EBI search and sequence analysis tools APIs in 2019. *Nucleic Acids Res.* 10.1093/nar/gkz268
57. Brinkmann, V., Laube, B., Abu Abed, U., Goosmann, C., and Zychlinsky, A. (2010) Neutrophil Extracellular Traps: How to Generate and Visualize Them. *J. Vis. Exp.* **31**, 1325–7

Footnotes

This study was made possible in part by The Netherlands Organisation for Scientific Research (NWO; VIDI 723.013.009 and Aspasia 015.010.005 to ID). Further financial support for the appointment of ACA was from the Landsteiner Foundation for Blood Transfusion Research (LSBR No. 1638 to RRK).

The abbreviations used are: CXCL8, chemokine (C-X-C motif) ligand 8; CXCL81 chemokine (C-X-C motif) ligand 1; CXCR2, CXC chemokine receptor 2; GPCRs, G protein-coupled receptors; GAGs, glycosaminoglycans; CRS1, chemokine recognition site 1; CRS2, chemokine recognition site 2; CKBPs, chemokine-binding proteins; SPPS, solid phase peptide synthesis; PMN, polymorphonuclear neutrophil;

Experimental constraints	
Long	222
Medium [1 < (i-j) < 5]	75
Sequential [(i-j) = 1]	197
Intraresidue [i=j]	342
Total	836
Dihedral angle constraints	50
Number of restrains per residue	22.2
Number of long-range restrains per residue	5.6
Average atomic RMSD to the mean structure (Å)	
Backbone	0.6
Heavy atoms	1.1
Global quality scores (mean/Z score)	
Verify3D	0.47/0.16
Prosall	0.48/-0.70
PROCHECK (ϕ–ψ)	-0.33/-0.98
PROCHECK (all)	-0.36/-2.13
MolProbity clash score	1.75/1.23
Ramachandran statistics (% of all residues)	
Most favoured	88.2
Additionally allowed	9.5
Generously allowed	2.3
Disallowed regions	0.0

Table 1. Overview of NMR restraints and XPLOR refinement statistics determined for tEv3 17-56.

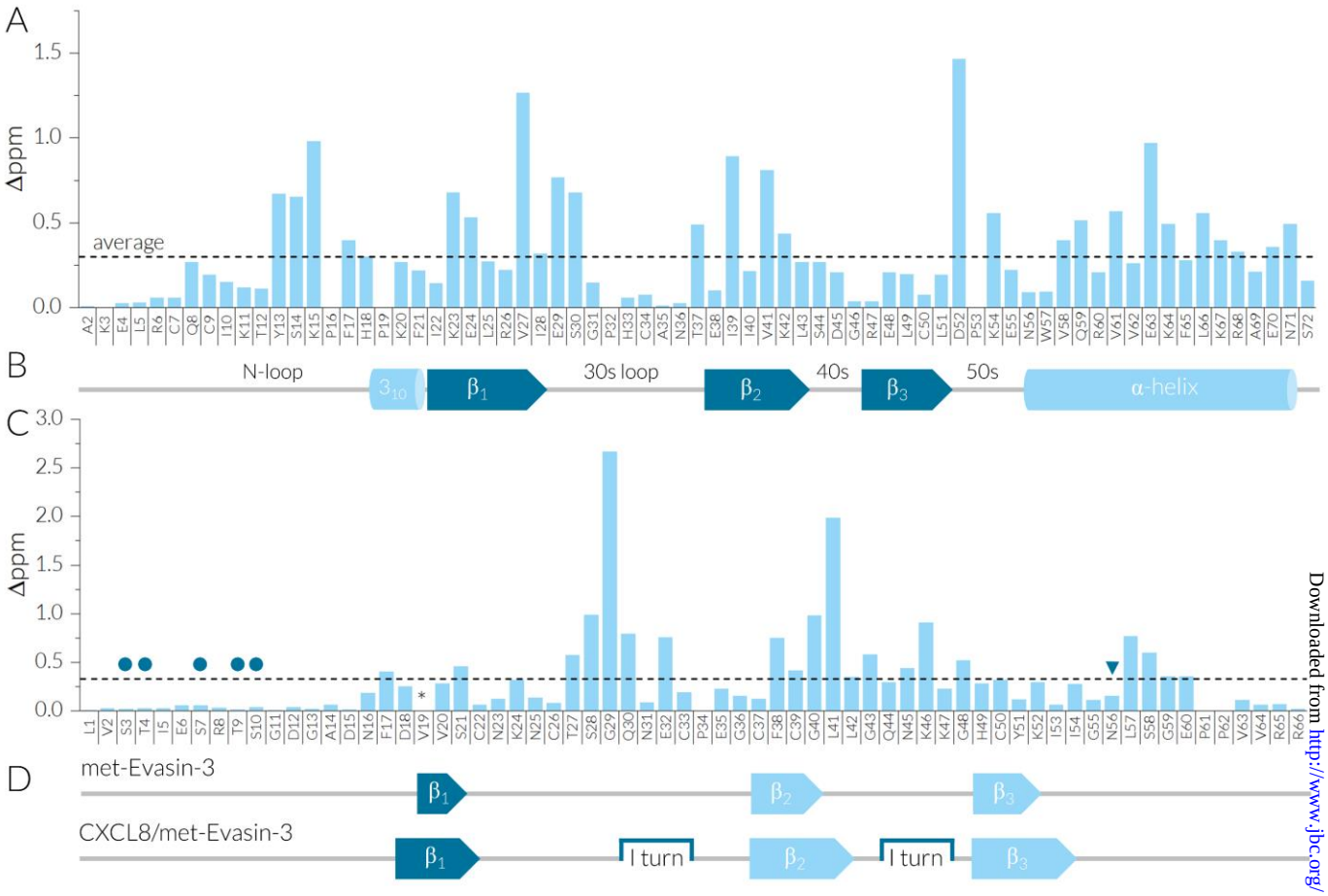

Figure 1. NMR analysis of binding CXCL8 to met-Evasin-3. **A.** The chemical shift perturbation plot of 200 μM [^{15}N, ^{13}C] CXCL8 amide peaks upon binding of 200 μM met-Evasin-3 at 37°C, pH 4.5. **B.** Schematic representation of CXCL8 secondary structure according to the dimer crystal structure (PDB ID: 1IL8). **C.** The chemical shift perturbation plot of 200 μM [^{15}N, ^{13}C] met-Evasin-3 amide peaks upon binding of 200 μM CXCL8 at 44°C, pH 4.5. Predicted O-glycosylation sites are marked by circles, N-glycosylation – by triangles. **D.** Schematic representation of met-Evasin-3 secondary structure predicted by CSI 3.0 in the unbound form (top) and in the complex with CXCL8 (bottom). Edge β-strands are shown by dark blue arrows, interior β-strands – by light blue arrows, turns – by square brackets. Δppm values are expressed as the sum of square roots $\left(\Delta 15N_{free-complex}\right)^2/6.51 + \left(\Delta 1H_{free-complex}\right)^2$

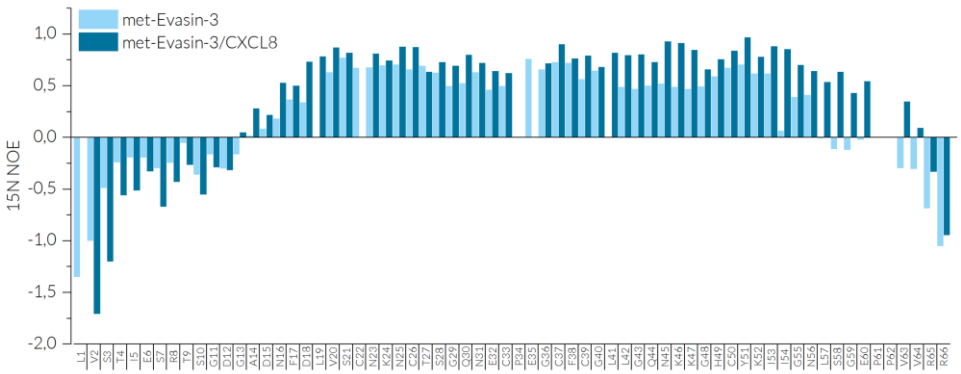

Figure 2. ^{15}N heteronuclear NOE relaxation values of [^{15}N, ^{13}C] met-Evasin-3 in free form (light blue) and in the CXCL8/[^{15}N, ^{13}C] met-Evasin-3 complex (dark blue).

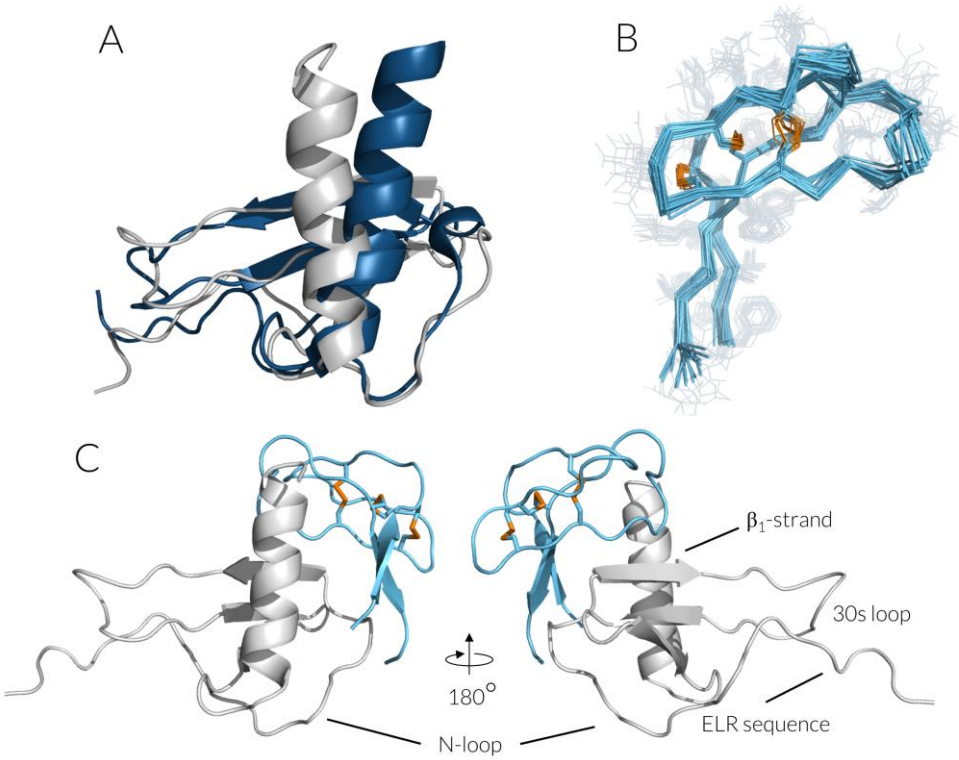

Figure 3. A. Overlay of CXCL8 structures in the CXCL8 dimer (dark blue; PDB ID 1IL8) and in the [^{15}N, ^{13}C] CXCL8/met-Evasin-3 complex (grey). **B.** Ribbon representation of the ensemble of 10 lowest energy structures of tEv3 17-56 (PDB ID: 6QJB); disulfides are shown by yellow sticks. **C.** Cartoon representation of the HADDOCK structure of the CXCL8/tEv3 17-56 complex. tEv3 17-56 is shown in light blue, CXCL8 – in grey.

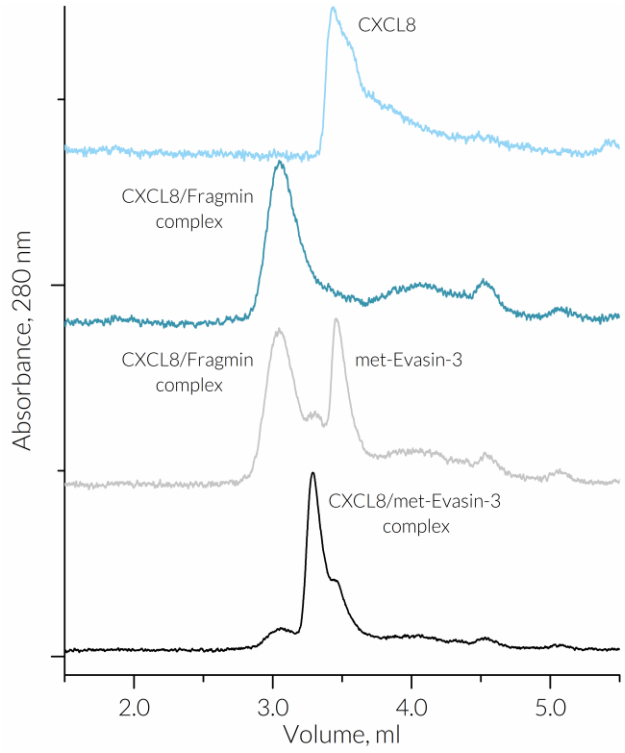

Figure 4. Chromatographic elution profiles of 0.1 mg/ml CXCL8 in absence (light blue) and presence (dark blue) of 1 mg/ml of low molecular weight heparin (Fragmin). SEC chromatograms taken immediately after addition and after 1-hour incubation at 37°C with 0.1 mg/ml met-Evasin-3, depicted in grey and black, respectively.

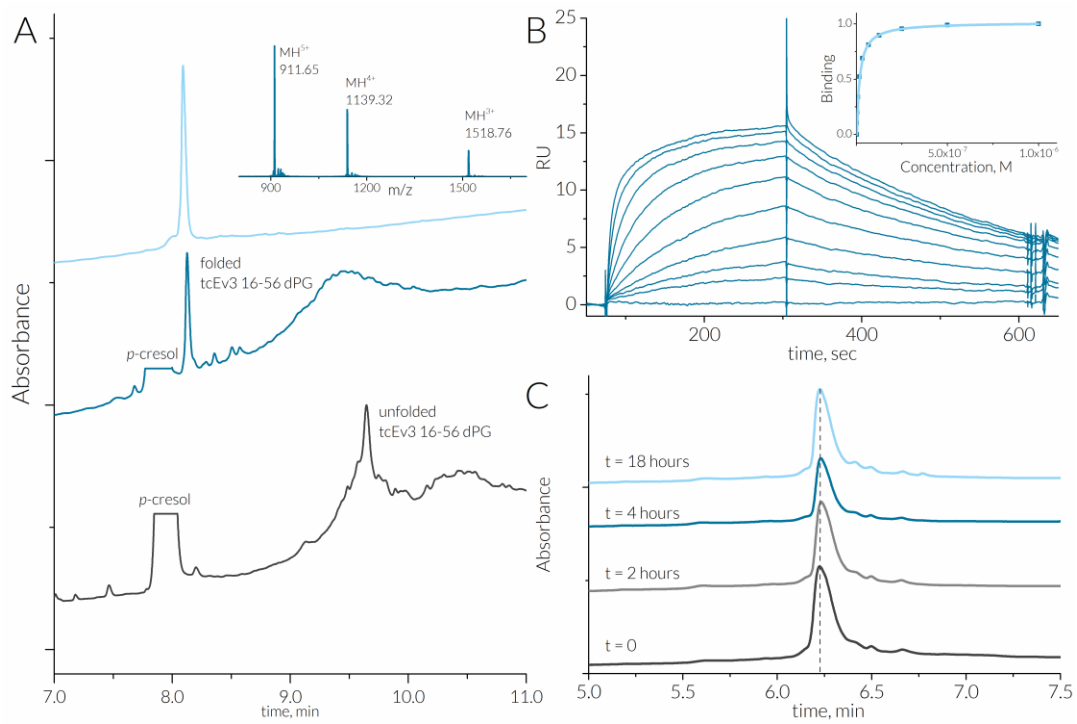

Figure 5. A. Overview of tcEv3 16-56 dPG folding and purification. The chromatograms of crude peptide mixture after HF cleavage and after folding are shown in black and dark blue, respectively. Results of the LC-MS analysis of purified tcEv3 16-56 dPG is shown in light blue; the calculated mass of $[MH]^+$ is 4552.02 Da, observed – 4552.06 Da. **B.** SPR biosensor analysis of tcEv3 16-56 dPG upon binding to immobilized human CXCL8. The binding curve is plotted using maximal response signal for each injection. Apparent Kd value is calculated by fitting the data to a steady-state affinity model using a linear component. The fitted Kd is 13 nM, R_{max} = 16.4, Chi^2 = 0.202. **C.** HPLC analysis of stability of tcEv3 16-56 dPG in human plasma at 37°C.

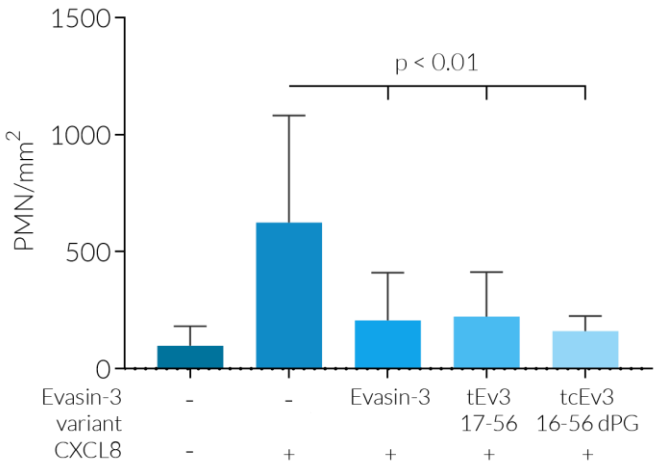

Figure 6. Effect of Evasin-3 variants on CXCL8 induced PMN migration. Indicated are PMN migration as a result of addition of 1 nM CXCL8 (n = 10) compared to the control without chemoattractant (n = 10) and compared to the effect of 10 nM Evasin-3 (n = 10); tEv3 17-56 (n = 9), or tcEv3 16-56 dPG (n = 5) on CXCL8 induced PMN migration.

Tick saliva protein Evasin-3 modulates chemotaxis by disrupting CXCL8 interactions with glycosaminoglycans and CXCR2

Stepan S. Denisov, Johannes H. Ippel, Alexandra C.A. Heinzmann, Rory R. Koenen, Almudena Ortega-Gomez, Oliver Soehnlein, Tilman M. Hackeng and Ingrid Dijkgraaf

J. Biol. Chem. published online June 24, 2019
